Shap. Mem. Superelasticity (2021) 7:314–332
https://doi.org/10.1007/s40830-021-00325-2

TECHNICAL ARTICLE

Thermomechanical Behavior of NiTi-8Hf Low-Temperature Shape Memory Alloys

O. Benafan[1] · G. S. Bigelow[1] · A. Garg[1,2]

Received: 28 January 2021 / Revised: 1 March 2021 / Accepted: 5 March 2021 / Published online: 7 May 2021

Abstract The actuation response of NiTi-8Hf alloys with low transformation temperatures was investigated. Four alloys with Ni-rich compositions of $Ni_{50.3}Ti_{41.7}Hf_8$, $Ni_{51}Ti_{41}Hf_8$, $Ni_{51.5}Ti_{40.5}Hf_8$, and $Ni_{52}Ti_{40}Hf_8$ (at.%) were melted, and subjected to several aging heat treatments between 450 and 550 °C. Transmission electron microscopy revealed the presence of H-phase precipitates, which varied in shape and size as a function of Ni content and aging condition. When aged at 550 °C for 3 h, the lowest Ni-containing alloy showed a preferential heterogeneous distribution of the H-phase precipitates with elongated lenticular shapes, while higher Ni resulted in a uniform distribution of less elongated particles. Uniaxial constant force thermal cycling experiments were used to reveal the shape memory properties of each alloy. In many aged conditions, no transformation peaks were observable in the DSC data. This absence of peaks in the DSC is attributed to the compounded effects of suppressed martensitic transformation due to higher off-stoichiometric Ni, and the strain fields around the precipitates that prevent transformation under stress-free cycling. However, these effects can be overcome by undercooling or thermally cycling under an applied stress. Thus, fully developed hysteresis loops were observed in the thermomechanical data for all aging conditions. The shape memory effect in compression showed maximum recoverable transformation strains of 3.7% in the lowest Ni containing alloy, which decreased with the addition of Ni to 1.7% in the 52Ni alloy. Inversely, the dimensional stability improved with added Ni, showing nearly zero residual strain in the higher Ni-containing alloys for stresses as high as 1 GPa.

Keywords NiTiHf · Shape memory alloy · H-phase · Actuation

Introduction

For more than a decade, NiTiHf shape memory alloys (SMAs) have been primarily examined for two target applications—high temperature actuation [1], and tribology [2–4]. The majority of the high temperature SMAs for actuation consist of compositions with less than 50.5 at.% Ni and 15 to 30 at.% Hf, while the NiTiHf superelastic alloys for tribology applications are limited to small amounts of Hf on the order of 1–3 at.% in a very Ni-rich matrix (54–55 at.%). These two alloy categories have been matured from laboratory-scale research to components and devices [5–7], and are now commercially produced and marketed. Only recently, this NiTiHf alloy family has also been considered for medical devices [8, 9] and low temperature actuation (below 0 °C) [10, 11].

In the Ti–rich and stoichiometric alloys, a steady increase in transformation temperatures is typically observed with the addition of Hf, where temperatures remain mainly above 0 °C and can go as high as 622 °C [12]. However, the Ni-rich compositions display a dip in transformation temperatures around 5–10 at.% Hf, which gets more severe with higher Ni contents [10, 13, 14]. This latter category exhibits transformation temperatures in the sub-zero range [10, 14], and displays a minima around 8 at.%. Other chemistries such as Ni-rich binary NiTi or ternary compositions such as NiTiFe or NiTiNb also

✉ O. Benafan
othmane.benafan@nasa.gov

[1] Materials and Structures Division, NASA Glenn Research Center, Cleveland, OH 44135, USA

[2] University of Toledo, Toledo, OH 43606, USA

exhibit transformation temperatures below 0 °C, but the temperatures continue to decrease with added Ni [15], or Fe and Nb in the case of ternary alloys. Based on the established properties of NiTiHf in the high temperature range or superelastic range as described above, the minimum in the NiTiHf transition temperatures can be expected to render benefits in various low-temperature actuator applications and, thus, warrants further investigation.

Historically, NiTiHf alloys with 8 at.% Hf content have been studied by numerous researchers dating back several decades, mainly focusing on Ti–rich or stoichiometric formulations. Early reports by AbuJudom et al. [16] and Angst et al. [12] examined Ti–rich $Ni_{49}Ti_{51-x}Hf_x$ (at.%) alloys, where the 8Hf composition exhibited an austenite peak temperature of 156 °C. Potapov et al. [17] examined melt-spun $Ni_{49.8}Ti_{50.2-x}Hf_x$ (at.%) using X-ray diffraction and resistivity measurements, and reported an austenite finish temperature of 142 °C for the 8Hf alloy. Similarly, Dalle et al. investigated the same composition ($Ni_{49.8}Ti_{42.2}Hf_8$) produced via induction melting to make cigar shapes [18] and twin roll casting to make strips [19]. The actuation response of this Ti–rich $Ni_{49.8}Ti_{42.2}Hf_8$ alloy was first studied by Kockar et al. [20] and Simon [21] while assessing the effect of severe plastic deformation via equal channel angular extrusion on the thermomechanical response. Wojcik [22] conducted work on a stoichiometric composition of $Ni_{50}Ti_{42}Hf_8$ produced using non-consumable vacuum arc melting. He showed the potential of processing these alloys with useful shape memory properties. Tong et al. [23] examined $Ti_{49}Ni_{51-x}Hf_x$ alloys with Hf contents from 3 to 15 at.%, and determined transformation temperatures, which for alloys with 7 and 10 at.% Hf exhibited austenite peak temperatures between 160 and 230 °C. König et al. [24] used high-throughput experimentation techniques to produce $Ni_{47}Ti_{45}Hf_8$ and $Ni_{48}Ti_{44}Hf_8$ thin films, among others, and in their study, the 8Hf alloy showed an austenite finish temperature near 70 °C. Amin-Ahmadi et al. [9, 25] investigated a slightly Ni-rich $Ni_{50.3}Ti_{49.7-x}Hf_x$ ($x \leq 9$ at.%) and reported on the aging effects and the role of the H-phase precipitates on mechanical stability and strength. Soares et al. [26] reported on $Ni_{50}Ti_{50-x}Hf_x$ (x = 8, 11, 14, 17 and 20 at. %) alloys, where the 8Hf alloy showed an austenite finish temperature near 115 °C.

While these and other reports (summarized in Table 1) have considered the 8Hf alloys in some capacity, the potential of NiTi-8Hf alloys for actuation applications at temperatures below ambient has not been explored. Moreover, the majority of these previous studies were on Ni-lean or stoichiometric alloys that had no potential for precipitate strengthening. Only in recent studies of Ni-rich NiTi-8Hf formulations [9, 25], has the role of precipitation strengthening via the nanoscale H-phase precipitates been explored. Hence, the current work was undertaken to embark on examining actuation potential of precipitation strengthened Ni-rich NiTi-8Hf low-temperature alloys. Four Ni-rich alloys (50.3, 51, 51.5 and 52 at.% Ni) were produced and evaluated for this purpose. The shape memory properties were assessed using differential scanning calorimetry (DSC), hardness and thermomechanical testing, and the microstructures were evaluated using transmission electron microscopy (TEM).

Experimental Methods

Four Ni-rich alloys with a nominal (target) composition of $Ni_{50.3}Ti_{41.7}Hf_8$, $Ni_{51}Ti_{41}Hf_8$, $Ni_{51.5}Ti_{40.5}Hf_8$, and $Ni_{52}Ti_{40}Hf_8$ (at.%) were produced from high purity elements. The 51-52Ni alloys were vacuum arc melted (VAM) in a water-cooled copper crucible under an argon atmosphere using a non-consumable tungsten electrode (alloys designated C16-C18). For these alloys, a starting charge of 50 g was melted, inverted and re-melted five times to ensure complete mixing. The resulting buttons were then homogenized in vacuum at 1050 °C for 24 h and gas quenched. The 50.3Ni alloy was vacuum induction melted (VIM) in a graphite crucible with a starting weight of approximately 600 g. The molten metal was cast into a 25.4 mm diameter ingot, which was vacuum homogenized at 1050 °C for 72 h and furnace cooled. The ingot was then extruded at 900 °C with an area reduction ratio of 7:1 (alloy designated E266).

Cylindrical test specimens from the extruded rod and buttons were fabricated using wire electrical discharge machining, followed by centerless grinding to the desired final diameters. Heat treatments were performed in a tube furnace with flowing argon using various temperatures and times as shown in Table 2. During these aging heat treatments, specimens were double wrapped in tantalum foil to limit oxidation. For brevity, heat treatments will be denoted using a short hand notation of temperature, time and cooling method (e.g., 550 °C/3 h/AC, refers to a sample heat treated at 550 °C for 3 h and air cooled), with the exception of two-step heat treat #4 (300 °C/12 h/AC + 550 °C/0.5 h/AC), which will be designated as 550 °C/0.5 h/AC in the following sections.

Differential scanning calorimetry (DSC) samples consisted of 5 mm diameter disks which were 1 mm thick. Measurements were performed using a TA Instruments Q1000 with a heating/cooling rate of 10 °C/min. Each specimen was cycled multiple times between − 150 and 110 °C. Hardness measurements were conducted on mechanically polished 5 mm diameter samples using a Struers DuraScan automated Vickers microhardness tester with 1 kgf load applied for 13 s.

Table 1 Summary of NiTi-8Hf (at.%) alloys investigated. It is noted that this table represents the majority of prior work, but may not be inclusive of all works not found

Year	Authors	Reference #	Composition (at.%)	As (°C)	Af (°C)	Ms (°C)	Mf (°C)
1992	AbuJudom et al.*	[16]	$Ni_{49}Ti_{43}Hf_8$	–	156	86	–
1994	Tuominen		$Ni_{49.9}Ti_{42.1}Hf_8$		–	–	–
1995	Angst et al.	[12]	$Ni_{49}Ti_{43}Hf_8$	–	162	87	–
1997	Potapov et al.	[17]	$Ni_{49.8}Ti_{42.2}Hf_8$	111	142	69	50
2002	Dalle et al.**	[18]	$Ni_{49.8}Ti_{42.2}Hf_8$	111	141	74	49
2003	Dalle et al.***	[19]	$Ni_{49.8}Ti_{42.2}Hf_8$	112	145	76	52
2006	Kockar et al.	[20]	$Ni_{49.8}Ti_{42.2}Hf_8$	122	164	94	70
2006	Simon	[21]	$Ni_{49.8}Ti_{42.2}Hf_8$	118	157	90	65
2009	Wojcik	[22]	$Ni_{50}T_{i42}Hf_8$	94	138	72	43
2011	König et al.	[24]	$Ni_{47\text{-}48}Ti_{45\text{-}44}Hf_8$	range			
2015	Frenzel et al.	[15]	$Ni_{49.8}Ti_{42.2}Hf_8$	145	175	111	83
2018	Amin-Ahmadi et al.	[9]	$Ni_{50.3}Ti_{41.7}Hf_8$	1	13	-65	-73
2019	Soares et al.	[26]	$Ni_{50}Ti_{42}Hf_8$	55	115	46	6
2019	Benafan et al.	[10]	$Ni_{51\text{-}52}Ti_{41\text{-}40}Hf_8$	–	–	–	(-139 to -95)
2020	Mills et al.	[4]	$Ni_{50.3\text{-}56}Ti_{41.7\text{-}36}Hf_8$	–	–	–	–
2021	Benafan et al.	This work	$Ni_{50.3\text{-}52}Ti_{41.7\text{-}40}Hf_8$	range			

*Ap and Mp values: refer to original work for more details

**30th cycle: refer to original work for more details

***Average value: refer to original work for more details

Table 2 Heat treatment temperatures and times used in this work

Heat treatment		$Ni_{50.3}Ti_{41.7}Hf_8$ (at.%)	$Ni_{51}Ti_{41}Hf_8$ (at.%)	$Ni_{51.5}Ti_{40.5}Hf_8$ (at.%)	$Ni_{52}Ti_{40}Hf_8$ (at.%)
HT1	1050 °C/24-72 h/GQ		×	×	×
HT2	450 °C/10 h/AC	×	×	×	×
HT3	500 °C/5 h/AC	×	×	×	×
HT4	300 °C/12 h/AC + 550 °C/0.5 h/AC		×	×	×
HT5	550 °C/1 h/AC	×	×	×	×
HT6	550 °C/3 h/AC	×	×	×	×

GQ = Gas quenched, *AC* = Air cooled

Transmission electron microscopy (TEM) specimens consisted of 3 mm diameter disks that were mechanically ground to ~ 130 µm thickness, and then electro-polished using a solution of 20% H_2SO_4 and 80% methanol (by volume) cooled to − 5 °C in a Struers Tenupol-5 twin-jet electropolisher. TEM images and diffraction patterns were collected at room temperature using a double tilt holder in a FEI Talos F200S STEM/TEM microscope operating at 200 kV.

Uniaxial constant force thermal cycling (UCFTC) experiments were conducted in an MTS 810 servo-hydraulic load frame. Specimens, of 5 mm diameter and 10 mm long, were thermally cycled between lower and upper cycle temperatures of − 65 and 150 °C at constant stresses from 0 to − 1300 MPa in compression. Cooling was accomplished using a liquid nitrogen assisted refrigerated environmental chamber for achieving a constant ambient temperature of near − 70 °C, while heating was accomplished using an induction heater with coils placed inside the chamber around the hot grips and platens. Strains were measured using an MTS contact extensometer with alumina extension rods. Thermomechanical tests were performed in series, with the sample loaded to a given stress, followed by two thermomechanical cycles. Then the load was increased to the next level and the sample thermally cycled again. Data from the second

thermomechanical cycle at each stress level were used to calculate the reported shape memory properties.

Results

Figure 1 shows a collection of DSC curves for the four NiTi-8Hf compositions after various heat treatments at different times and temperatures. For clarity, only the second DSC cycle is shown for each sample. In the homogenized condition (1050 °C/24 h/GQ), no transformation peaks were observed in any composition over the temperature range used (limited to − 150 °C on cooling). After aging, distinct martensitic transformation peaks appeared in some conditions, but were still absent in others. In the 50.3Ni alloy (Fig. 1a), aging at the lowest temperature of 450 °C/10 h prompted a very broad peak on heating, and an even broader and nearly undiscernible peak on cooling as shown in the inset of Fig. 1a. Raising the aging temperature to 500 °C/5 h promoted sharp and distinct transformation peaks on both heating and cooling. Aging at 550 °C for 1 and 3 h resulted in relatively broader peaks compared to the 500 °C aging but occurring at lower temperatures.

In the 51Ni alloy (Fig. 1b), no DSC peaks were observed, with the only exception being the sample aged at 550 °C/3 h. For this condition, the transformation peaks exhibited an asymmetric enthalpy reaction where the peak on heating was sharper than the peak on cooling, and displayed a very wide hysteresis of > 100 °C. The 51.5Ni alloy (Fig. 1c) exhibited clear transformation peaks when aged at 450 °C/10 h and 500 °C/5 h, with lower temperature peaks for the latter heat treatment. A very small and uncharacteristic peak was also observed in the 550 °C/3 h aged sample, but only on heating, as shown by the inset of Fig. 1c. This peak was found to be reproducible with cycling suggesting that a small amount of martensite might be forming on cooling, but with a very small and broad peak that cannot be easily identified. Finally, the 52Ni alloy (Fig. 1d) showed transformation peaks in all five aging conditions, with transformation temperatures decreasing as aging temperatures increased, and for the 550 °C aging conditions, transformation temperatures increased with increasing aging time.

Figure 2 displays a summary of the transformation temperatures taken from the second cycle DSC scans as a function of Ni content for the austenite start (A_s), austenite finish (A_f) martensite start (M_s), and martensite finish (M_f)

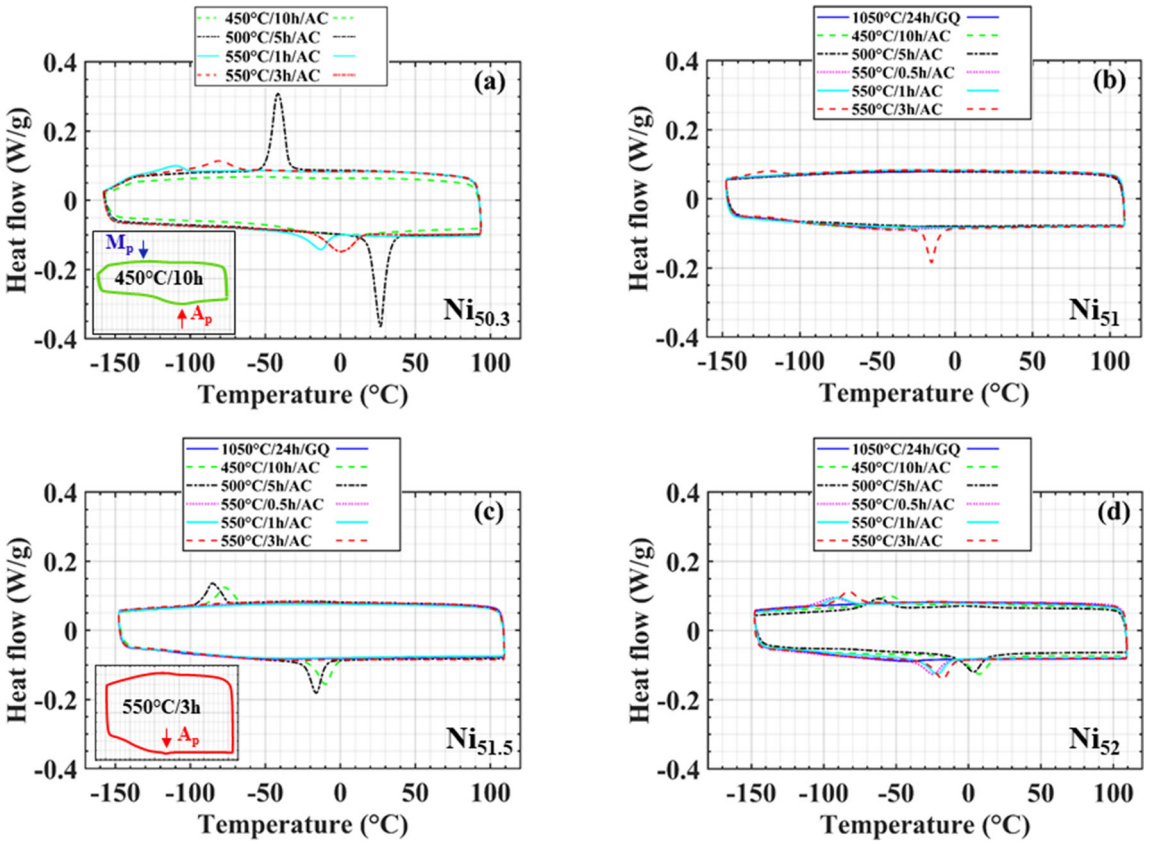

Fig. 1 Differential scanning calorimetry (DSC) measurements for different heat treatments corresponding to **a** $Ni_{50.3}Ti_{41.7}Hf_8$, **b** $Ni_{51}Ti_{41}Hf_8$, **c** $Ni_{51.5}Ti_{40.5}Hf_8$, and **d** $Ni_{52}Ti_{40}Hf_8$ (at.%) alloy. Only the second thermal cycle is shown

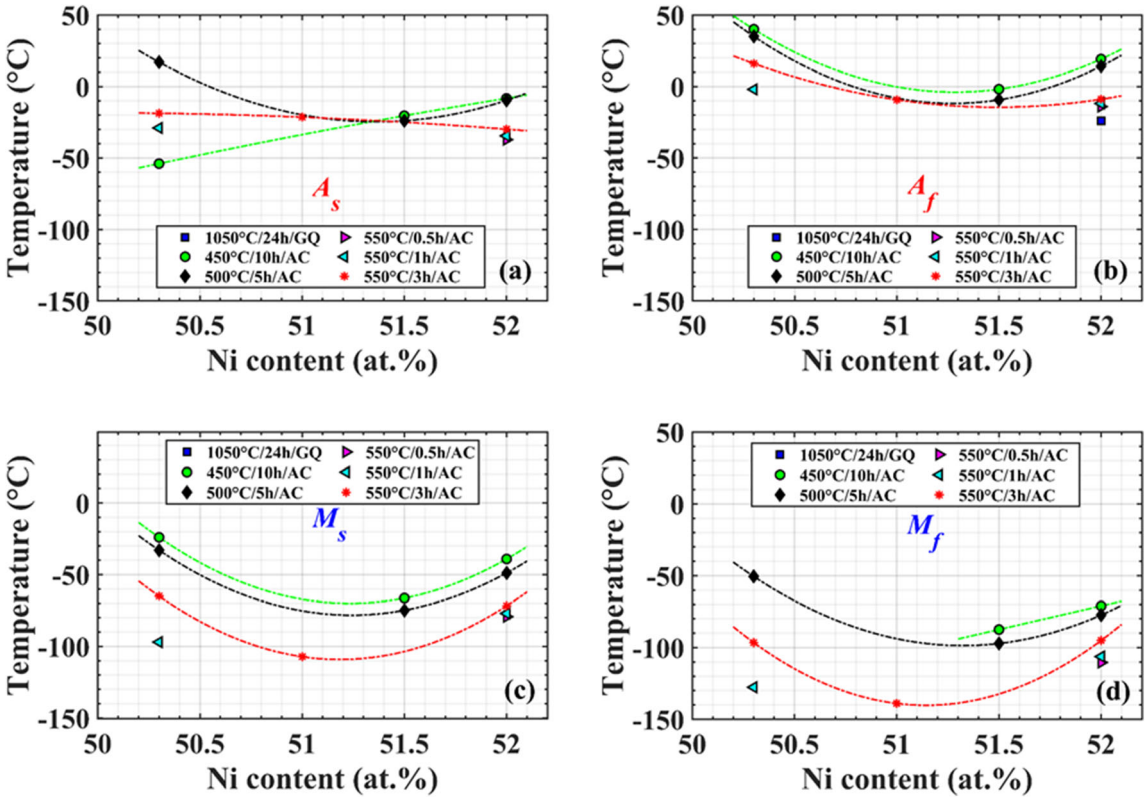

Fig. 2 Characteristic transformation temperatures **a** austenite start (A_s), **b** austenite finish (A_f), **c** martensite start (M_s), and **d** martensite finish (M_f) as a function of Ni content, corresponding to the second thermal cycle of the DSC data

temperatures. In addition to the pointwise data, fit lines were overlaid to help with data visualization and trends. For a given aging treatment, the general trend is that the transformation temperatures decrease with added Ni, reach a minimum between 51 and 51.5 at.% Ni, and then increase again at 52 at.% Ni. Overall, transformation temperatures decreased with increasing aging temperature (i.e., inverse relationship), such that the highest transformation temperatures were obtained after aging at 450 °C/10 h. However, for a given Ni content, it was observed that at the 550 °C aging temperature, the transformation temperatures increased with aging time (i.e., direct relationship), such that the lowest values were obtained after aging at 550 °C/0.5 h. The exception to this trend was the 50.3Ni alloy, which showed an A_s in the 450 °C/10 h condition lower than that for the 550 °C/1 h condition (Fig. 2a). Consequently, a wide range in transformation temperatures could be developed in a single composition using the various heat treatments, e.g. in the 50.3Ni alloy, M_s (Fig. 2c) varied from − 97 to − 24 °C, a change of 73 °C. It should be noted that in this alloy, the measured M_s temperature of − 65 °C in the 550 °C/3 h aging condition agrees well with the one obtained by the DSC study reported earlier in [25].

Vickers microhardness as a function of heat treatment is shown in Fig. 3. Each alloy was indented ten times at different locations and the mean, standard deviation, minimum and maximum values are reported in a boxplot format. When comparing the data across the Ni content, the lowest hardness values were recorded in the 50.3Ni alloy (Fig. 3a), while the highest values are observed for the 51.5Ni and 52Ni alloys (Fig. 3c-d). This is somewhat expected given that added Ni in solution and any ensuing second phase precipitates play a role in increasing the strength of the material. The effects of specific heat treatments are also apparent from these plots. The highest Vickers hardness number (VHN) in the 50.3Ni alloy (Fig. 3a) occurred after aging at 450 °C/10 h (HT2), with a mean of 373, followed by a drop in hardness when aged at higher temperatures. These values are lower than the previously reported values for the same alloy composition [4], but the difference may be attributed to solutionizing or the additional pre-aging heat treatment performed in [4] that may have raised the hardness. The 51Ni alloy (Fig. 3b) showed an increase in hardness from the homogenized condition (HT1) with the highest value obtained after aging at 450 °C/10 h (HT2), with a hardness of 534 VHN. Other aging treatments resulted in a slight decrease or similar values in some cases, when considering the data spread. Alloy 51.5Ni (Fig. 3c) exhibited the highest hardness in the homogenized condition (HT1) with a value of 584 VHN,

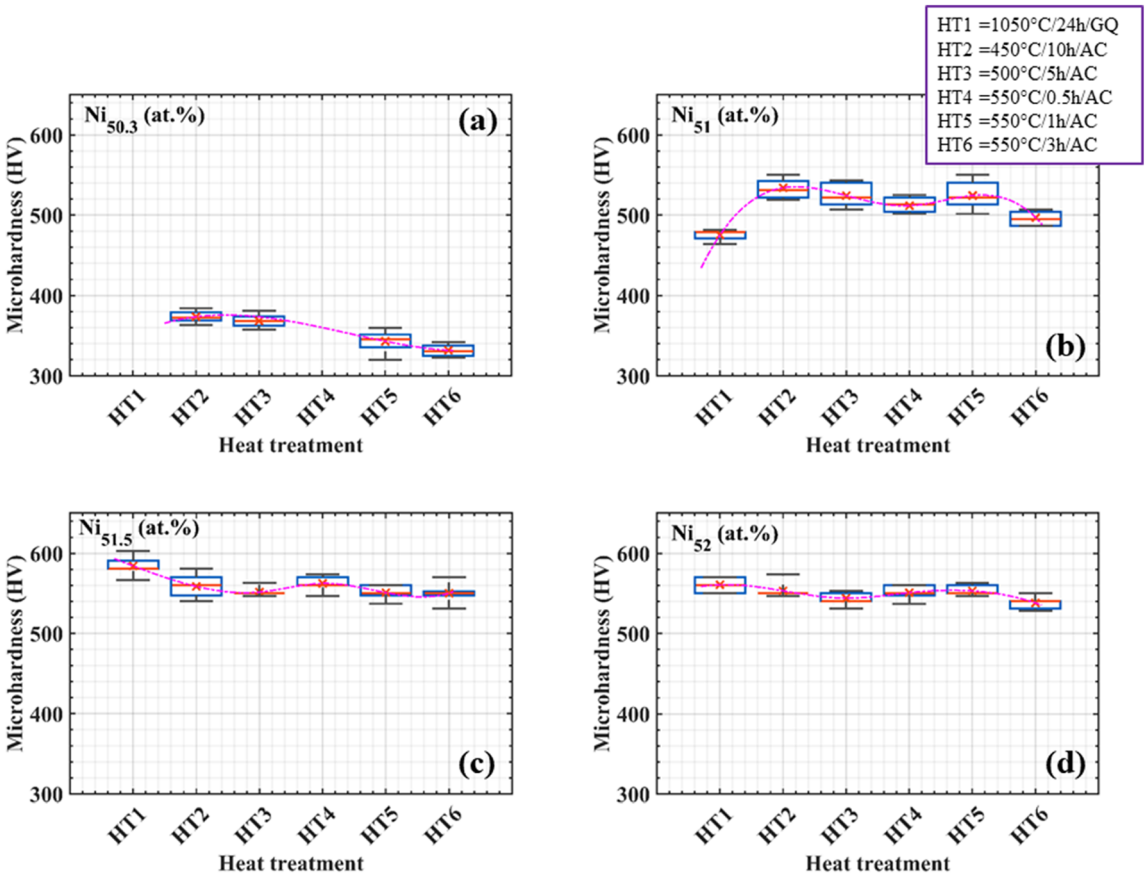

Fig. 3 Vickers microhardness as a function of heat treatments corresponding to **a** $Ni_{50.3}Ti_{41.7}Hf_8$, **b** $Ni_{51}Ti_{41}Hf_8$, **c** $Ni_{51.5}Ti_{40.5}Hf_8$, and **d** $Ni_{52}Ti_{40}Hf_8$ (at.%) alloy

followed by a slight decrease with aging. Finally, alloy 52Ni (Fig. 3d) also exhibited its highest value in the homogenized condition (HT1) with a mean hardness of 560 VHN that remained relatively unchanged by the subsequent aging conditions. For comparison purposes, these latter values are lower than previously reported values [4] of around 712 VHN on a similar alloy since their starting condition, aging temperatures and times, and potentially quench rates were different.

Figure 4 shows a series of TEM micrographs taken at room temperature for the 51Ni alloy. In the homogenized condition (Fig. 4a), the alloy consisted of single B2 austenite phase with a small amount of a secondary precipitate phase observed only near structural features. These precipitates are believed to have formed during cooling from 1050 °C, particularly at high-energy sites such as low-angle and sub-grain boundaries (shown in Fig. 4a), dislocations, or imperfections in grain boundaries, where atoms diffuse more rapidly. This precipitate phase was identified as the orthorhombic H-phase [27] via its characteristic 1/3, $2/3 < 110 >_{B2}$ extra spots (marked by arrows) in a $< 111 >_{B2}$ zone axis selected area diffraction pattern (SADP) shown in the inset of Fig. 4a. Aging at 450 °C/10 h (Fig. 4b) produced a high density of lenticular H-phase precipitates with a very fine and uniform distribution throughout the B2 matrix. The average precipitate size in this condition was estimated to be 12 nm. Aging at higher temperatures for different times resulted in similar microstructures, but with coarser H-phase precipitates reaching an approximate size of 25 nm for 550 °C/3 h heat treatment. This coarsening of the H-phase precipitates is clearly visible from 450 °C/10 h (Fig. 4b) to 550 °C/3 h heat treatment (Fig. 4f).

Figure 5 is a comparison of the TEM microstructures for all the alloys aged at 550 °C/3 h. This aging heat treatment was selected based on previous studies on similar alloys that provided the best overall shape memory properties. The presented micrographs are shown in multiple magnifications to better visualize the microstructures and the precipitate morphology, and to aid in comparison between the various compositions. In the 50.3Ni alloy (Fig. 5a1–a3), the low magnification images show a heterogeneous nucleation of the H-phase precipitates around dislocation structures, subgrain boundaries and intermittently within the grains. In this slightly Ni-rich composition, there is not enough driving force to nucleate the H-phase uniformly,

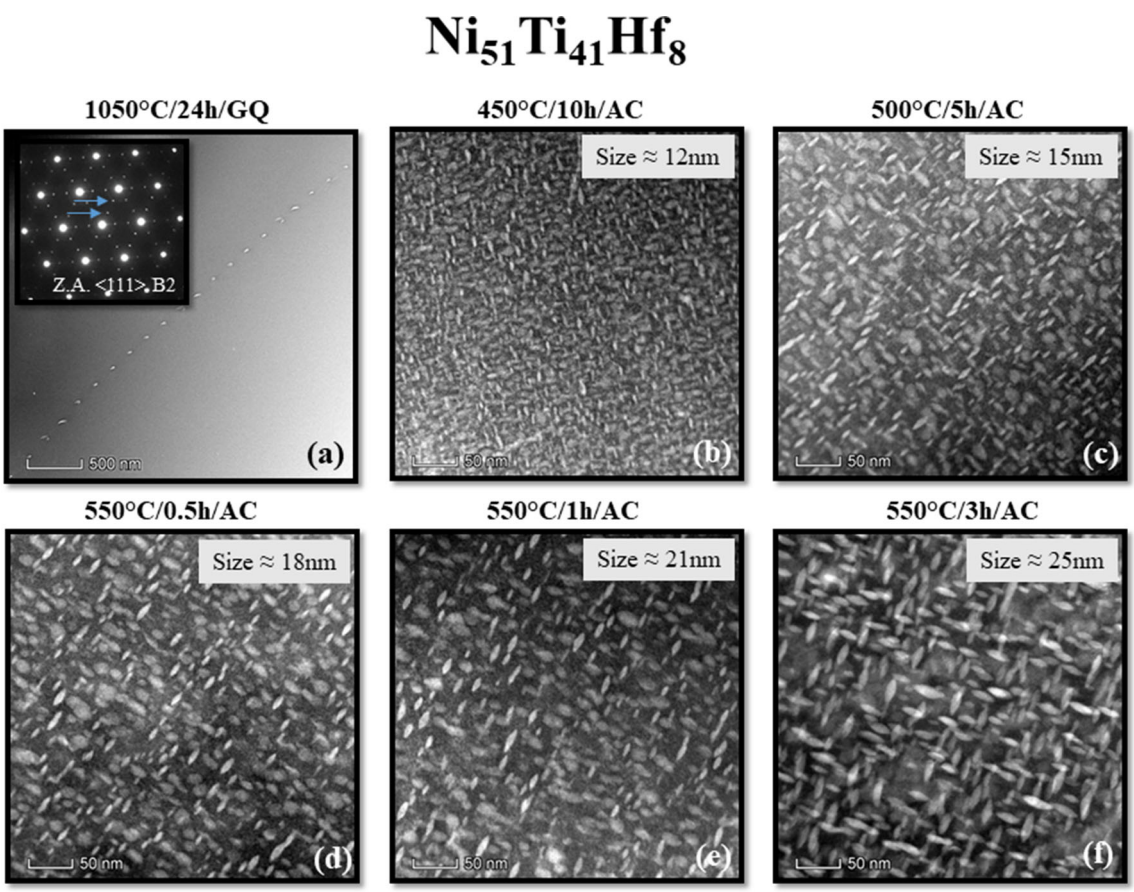

Fig. 4 Room temperature TEM micrographs for the $Ni_{51}Ti_{41}Hf_8$ alloy in different heat treatment conditions. **a** 1050 °C/24 h/GQ, **b** 450 °C/10 h/AC, **c** 500 °C/5 h/AC, **d** 550 °C/0.5 h/AC, **e** 550 °C/1 h/AC, and **f** 550 °C/3 h/AC. Inset of (**a**) represents a selected area diffraction pattern confirming the H-phase precipitates as indicated by the 1/3, 2/3 < 110 > B2 extra spots (arrows) in the < 111 > B2 zone axis. Precipitate average size (long dimension) are indicated on the top–right corner of the images

but rather only at energetically or chemically favored sites within the microstructure. This microstructure is consistent with similar low Hf-containing alloys aged at comparable temperatures and times [9]. The high magnification images show the overall shape of the H-phase precipitates within a grain having a lenticular (spindle-like) shape with an average size of 76 nm in the long direction and an aspect ratio of approximately 4.

The 51Ni alloy (Fig. 5b1–b3) formed a different microstructure after aging. Unlike the heterogeneous precipitation in the 50.3Ni alloy, the added Ni promoted homogeneous and uniform precipitation throughout the matrix. A higher volume fraction is observed with an average H-phase precipitate size of 25 nm. The higher Ni level in the 51.5Ni (Fig. 5c1–c3) and the 52Ni (Fig. 5d1–d3) resulted in similar homogeneous microstructures, with an increased average H-phase precipitate size of 40 and 68 nm, respectively. It is noted that the precipitate shape remained spindle-like but the aspect ratio decreased from 4 in the 50.3Ni to approximately 2 to 3 in the 51-52Ni, due to changes in the interfacial and elastic energies, which drive the particle shapes and the ensuing particle growth and coarsening.

Uniaxial constant force thermal cycling results for the four Ni compositions are shown in Fig. 6 through Fig. 9 for the different aging conditions. The strain-temperature data correspond to the 2nd thermal cycle at each stress level in compression, and it is provided to better visualize the macroscopic actuation response and the associated shape memory properties. In the 50.3Ni alloy (Fig. 6), a negligible response was obtained at 0 MPa, then the typical hysteresis loops developed at 100 MPa and higher stresses. Although aging at 450 °C/10 h resulted in very broad and nearly unmeasurable DSC peaks, the hysteresis shape of the thermomechanical response is clearly developed due to the applied stress. Similar observations are made for the 51Ni alloy (Fig. 7) where no DSC peaks were observed in most aging conditions. In the 51Ni alloy, however, higher stresses of greater than 200 MPa were required to produce a strain response for some aging conditions. The 51.5Ni (Fig. 8) and 52Ni (Fig. 9) alloys exhibited similar behavior

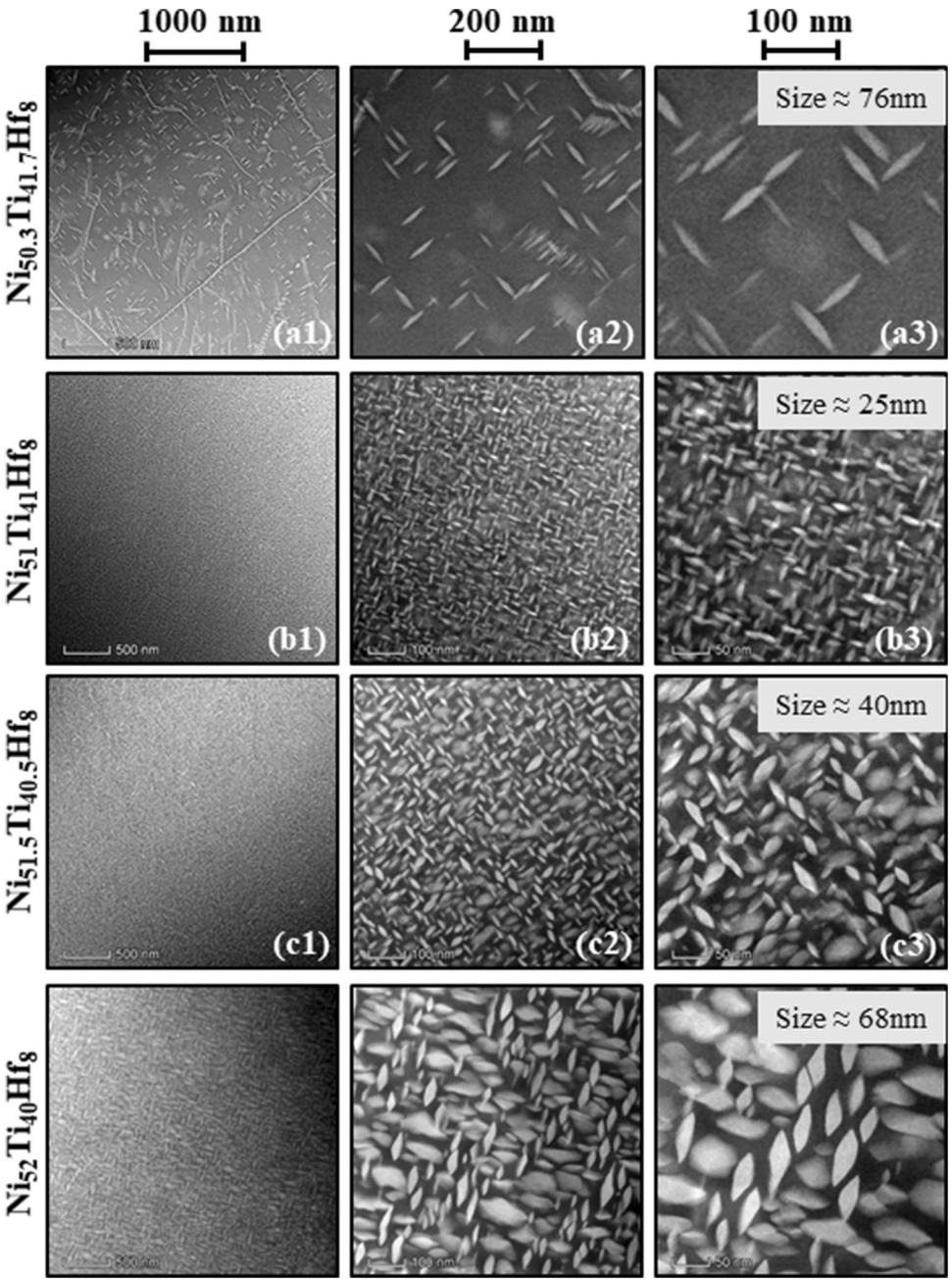

Fig. 5 Representative TEM micrographs of samples aged at 550 °C/3 h/AC with different magnifications. **a** $Ni_{50.3}Ti_{41.7}Hf_8$, **b** $Ni_{51}Ti_{41}Hf_8$, **c** $Ni_{51.5}Ti_{40.5}Hf_8$, and **d** $Ni_{52}Ti_{40}Hf_8$ (at.%) alloy. Precipitate average size (long dimension) are indicated on the top–right corner of the high magnifications images

irrespective of the presence or lack of DSC peaks in some aging conditions.

A summary of the transformation temperatures as a function of applied stress for the different alloys is shown in Fig. 10 through Fig. 13 for the various aging conditions. In the 50.3Ni alloy (Fig. 10), all temperatures increased linearly with increasing stress up to 800 MPa, above which the temperatures nearly leveled out, with the exception of A_f which kept on increasing with stress. For comparison with other alloys, 550 °C/3 h aging condition was chosen and the initial linear slope for the A_s was measured to be 0.13 °C/MPa in this alloy. The effect of aging followed a comparable trend to that observed in the DSC data where the highest transformation temperatures were obtained when aging was conducted at 500 °C/5 h. Although hysteresis loops for the 0 MPa stress case (or minimum stress of < 2 MPa to maintain contact between the platens and sample) were not visible in the thermomechanical data (no strain was measured), direct comparison with DSC is not entirely practical, given all DSC measurements are performed at zero applied stress. Moreover, the DSC curve corresponding to the 450 °C/10 h sample was very broad which makes interpretation of the characteristic temperatures somewhat challenging. For these reasons, the strain-

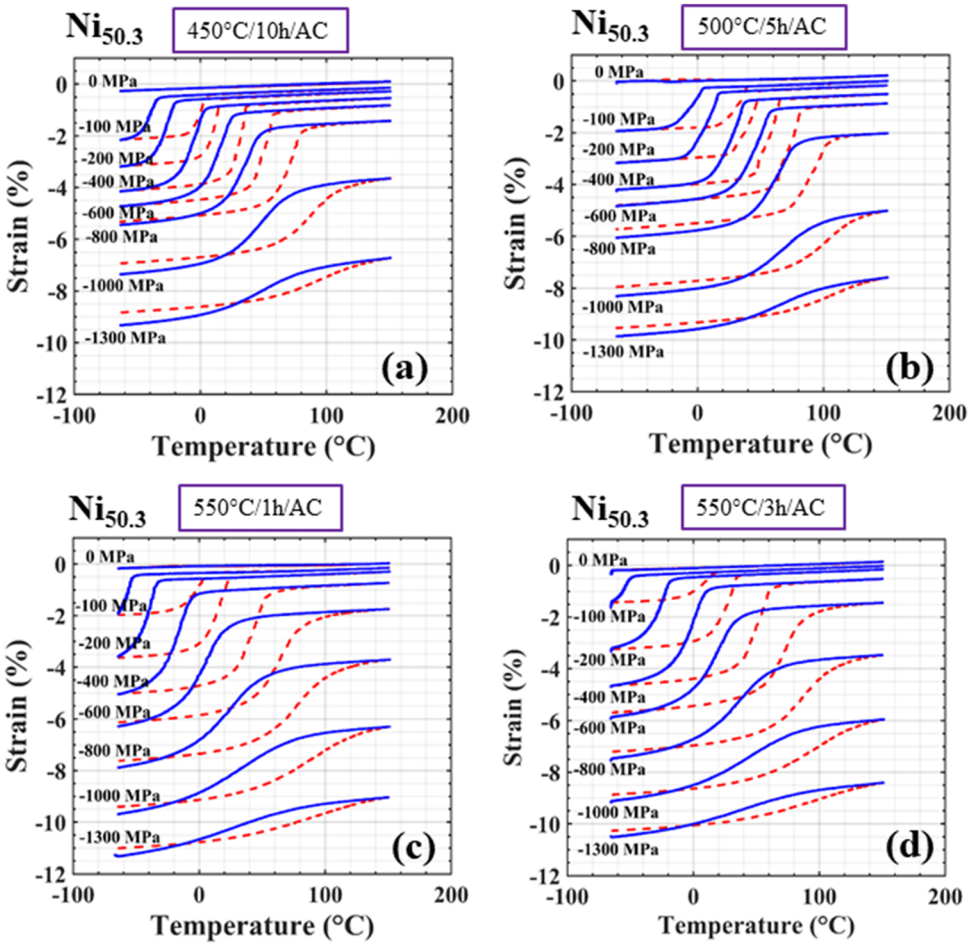

Fig. 6 Compressive constant force thermal cycling responses for the $Ni_{50.3}Ti_{41.7}Hf_8$ alloy aged at **a** 450 °C/10 h/AC, **b** 500 °C/5 h/AC, **c** 550 °C/1 h/AC, and **d** 550 °C/3 h/AC. Only the second cycle from some stress levels is shown

temperature data presented in Fig. 6 provide a better relationship between aging and the resulting transformation temperatures.

With added Ni, the transformation temperatures in the 51Ni alloy (Fig. 11) decreased compared to the 50.3Ni alloy, in agreement with the DSC data. Additionally, the temperature-stress sensitivity for all temperatures exhibited a linear relationship even at stresses as high as 1300 MPa, with a slope of 0.085 °C/MPa, measured at A_s in the 550 °C/3 h aged condition, compared to 0.13 °C/MPa for the 50.3Ni alloy. The highest temperatures in this alloy were obtained after aging at 550 °C/3 h, whereas the lowest temperatures were obtained at longer aging times of 450 °C/10 h, which did not follow the order observed in the 50.3Ni alloy.

The 51.5Ni (Fig. 12) and the 52Ni alloys (Fig. 13) exhibited an aging trend more analogous to their DSC data. Lower aging temperatures resulted in higher transformation temperatures, and for a given aging temperature, longer aging times also resulted in higher transformation temperatures. Similar to the 51Ni alloy, the temperature-stress sensitivity exhibited a linear relationship for all temperatures with measured slopes of the A_s in the 550°C/3 h aging condition of 0.074 and 0.064 °C/MPa for the 51.5Ni and 52Ni alloys, respectively. This trend suggests that increasing the Ni content decreases the temperature-stress sensitivity in these alloys.

The thermal hysteresis, measured as (A_f -M_s), as a function of applied stress is shown in Fig. 14 for all alloys. In the 50.3Ni alloy (Fig. 14a), the hysteresis varied with the different aging conditions, showing a decrease and then increase in the 450 °C/10 h and 500 °C/5 h aging treatments when evaluated from 0 to 1300 MPa. Referring back to the strain-temperature data of Fig. 6, it is clearly observed that the shape of the hysteresis loop changes with increasing stress. The slopes corresponding to the forward transformation (M_s to M_f) and the reverse transformation (A_s to A_f) are parallel and nearly vertical at low stresses, then become flatter at higher stresses, requiring a much higher temperature differential to complete the transformation. For example, the hysteresis in the 450 °C/10 h aged 50.3Ni alloy starts at 39 °C at 100 MPa, reaches a minimum of 32 °C at − 600 MPa, and then increases to 43 °C at 1300 MPa. The hysteresis for the 550 °C conditions behaved similarly, but were ∼ 25 °C higher overall than that for the 450 °C and 500 °C conditions, exhibited

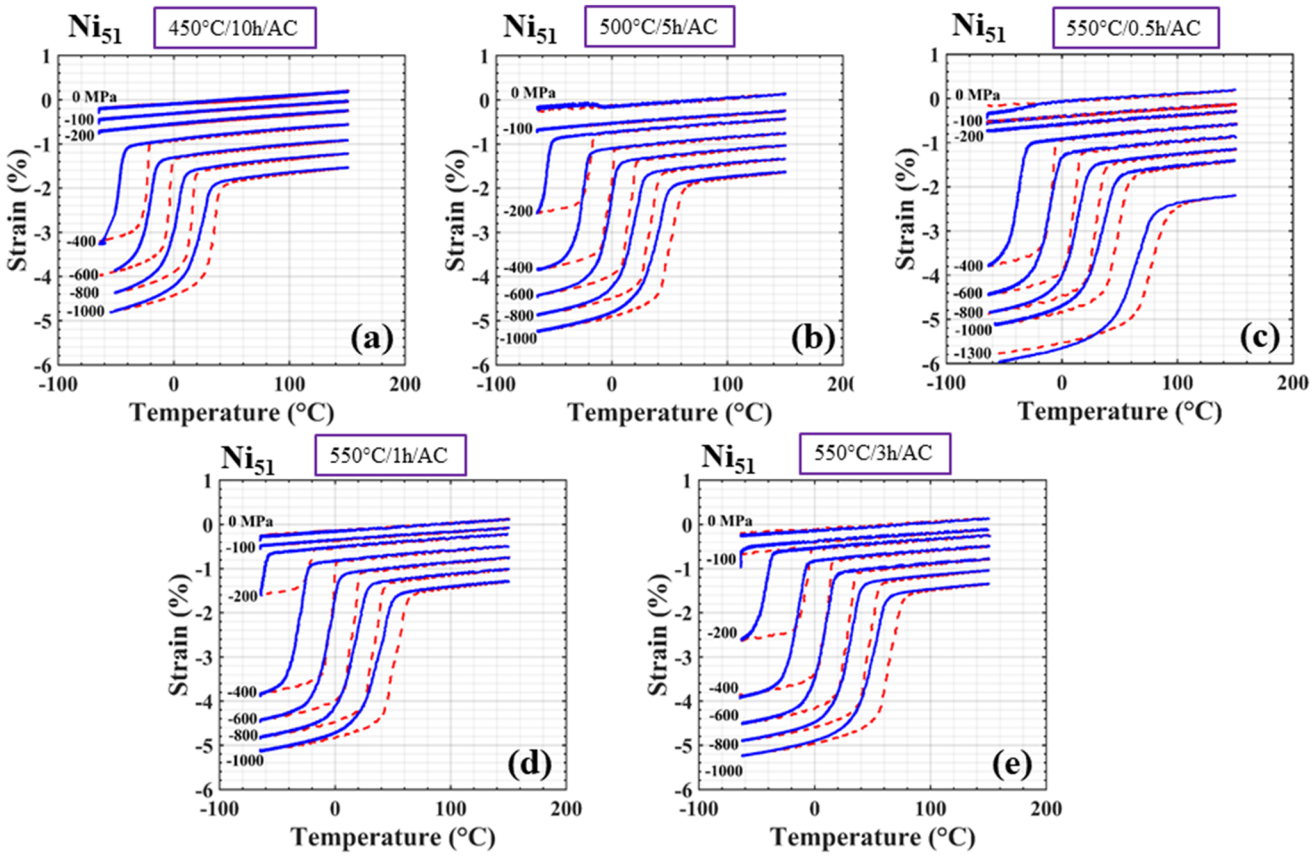

Fig. 7 Compressive constant force thermal cycling responses for the $Ni_{51}Ti_{41}Hf_8$ alloy aged at **a** 450 °C/10 h/AC, **b** 500 °C/5 h/AC, **c** 550 °C/0.5 h/AC, **d** 550 °C/1 h/AC, and **e** 550 °C/3 h/AC. Only the second cycle from some stress levels is shown

minimum values between 800 and 900 MPa, and increased at higher stresses.

A different hysteresis behavior is found in the 51Ni alloy as shown in Fig. 14b. The hysteresis decreases with added stress, with minimal effect from aging, having only about 10 °C difference from one aging treatment to another. The average hysteresis starts at 35 °C at 200 MPa then decreases to 13 °C at 1300 MPa. This behavior has been reported in similar alloys [28, 29], and is common in Ni-rich compositions. Similar behavior can also be observed in the hysteresis for the 51.5Ni (Fig. 14c) and the 52Ni (Fig. 14d) alloys.

The transformation strains as a function of applied stress are shown in Fig. 15 for all alloy compositions. The highest strains were obtained in the 50.3Ni alloy (Fig. 15a) with a maximum value of 3.7% at an applied stress of 500 MPa after aging at 550 °C/1 h. Other aging conditions such as the 450 °C/10 h and 500 °C/5 h exhibited slightly lower strains overall, but the maximum transformation strain for these conditions occurred at higher stresses of 700 MPa. Nonetheless, in all aging conditions, the transformation strain gradually decreased to ~ 1.5% at 1300 MPa after reaching their respective maximum value. The additional Ni in the 51Ni alloy (Fig. 15b) resulted in a different behavior as a function of stress. Unlike the 50.3Ni alloy, strain did not peak at an intermediate stress level, but rather gradually increased with stress in all aging conditions and asymptotically approached the highest strain of 3.1% at 1000 MPa in the 550 °C/3 h aged condition. Thus, while the maximum transformation strain was lower in the 51Ni, the alloy had significantly higher transformation strain capability at the higher stress levels. Similar observations were made for the 51.5Ni (Fig. 15c) and the 52Ni (Fig. 15d) alloys—noting that the overall strain magnitude decreased with added Ni, reaching a maximum of 2.3 and 1.7% in the 51.5Ni and 52Ni alloys, respectively. It is interesting to note that for the 52Ni alloy, the transformation strains at each applied stress level were almost the same, independent of the aging condition.

For a measure of dimensional stability, the residual strains in martensite are plotted as a function of applied stress in Fig. 16. In the 50.3Ni alloy, strain response is most stable after aging at 450 °C/10 h and 500 °C/5 h, which show nearly no residual strain up to 600 MPa. Then strains accumulate gradually with increased stress reaching near 0.5% at 1300 MPa. On the other hand, the other two

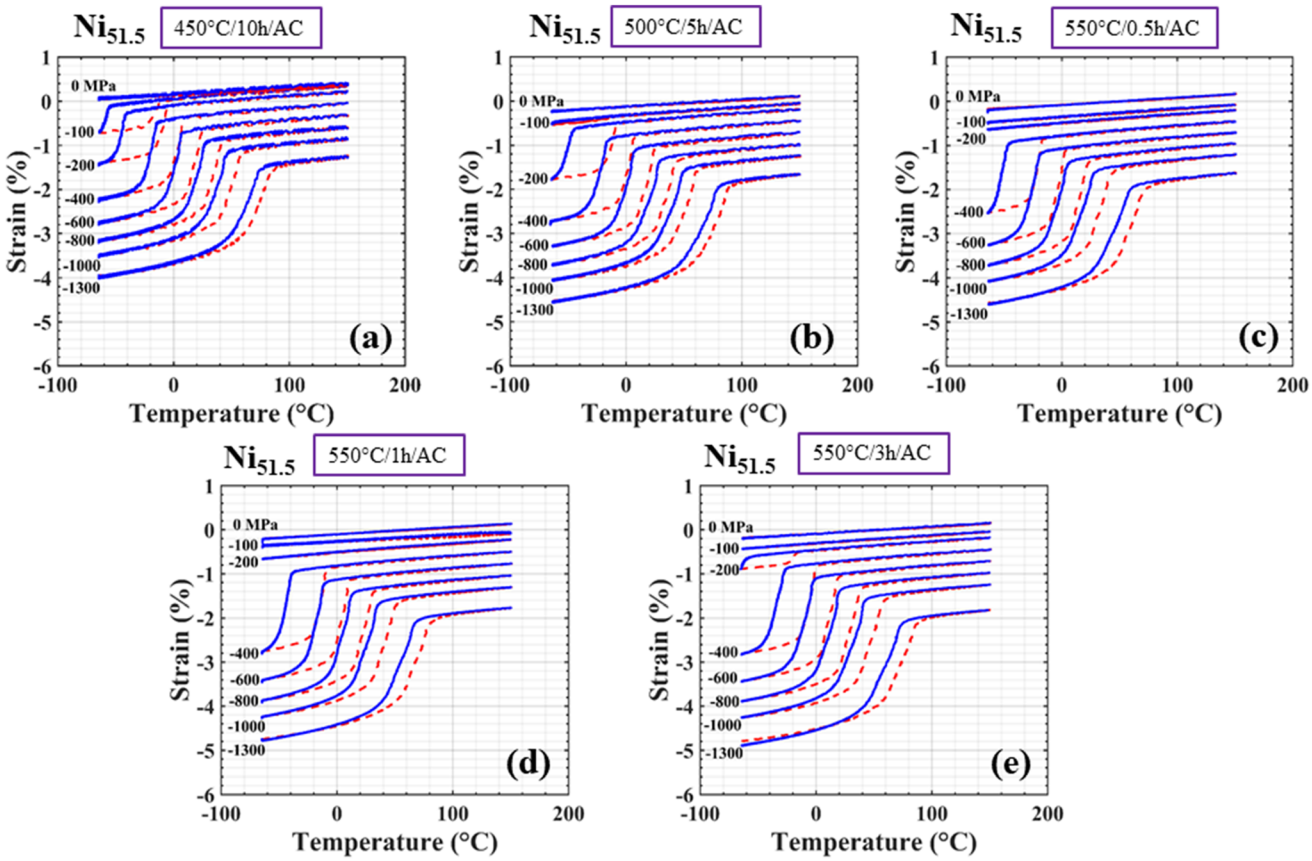

Fig. 8 Compressive constant force thermal cycling responses for the $Ni_{51.5}Ti_{40.5}Hf_8$ alloy aged at **a** 450 °C/10 h/AC, **b** 500 °C/5 h/AC, **c** 550 °C/0.5 h/AC, **d** 550 °C/1 h/AC, and **e** 550 °C/3 h/AC. Only the second cycle from some stress levels is shown

aging conditions (550 °C/1 h and 550 °C/3 h) exhibited a gradual increase in residual strains until leveling out at around 0.25% at maximum stress. The other three alloys shown in Fig. 16a–c exhibited a different, much more stable behavior with little to no residual strains up to stresses of 1000 MPa, followed by a small residual strain development of less than 0.25% at 1300 MPa in all cases.

Discussion

Similar to the Ni-rich NiTi alloys, shape memory and functional properties of the studied Ni-rich NiTi-8Hf alloys are shown to be influenced by the Ni content. Increasing levels of Ni lead to lowering and/or suppression of transformation temperatures, provide a potential for solid solution strengthening, and are the antecedent to the chemical driving force for precipitation. Furthermore, low amounts of Hf in Ni-rich NiTiHf alloys also lead to lower transformation temperatures [10, 13, 14], while the addition of Hf overall contributes to the driving force for precipitation and promotes the precipitation of H-phase instead of the Ni_4Ti_3 seen in binary NiTi. The results presented above are affected by one or a combination of these effects as discussed next.

The absence of enthalpy peaks in the DSC response under some aging conditions (Fig. 1) is frequently indicative of a lack of martensitic transformation. Such behavior has been commonly observed in cold worked alloys [30, 31] where deformed martensite along with processing-induced dislocations and point defects result in a broad transformation that is not detectable by the usual DSC peaks. Strain glass alloys [32, 33] have also been reported to have diminished DSC peaks due to disruption of the long-range strain ordering of the martensitic transformation, resulting in martensite nano-domains with a glass transition. This has been reported in NiTi-based alloys [34] and other material systems [35]. However, in the current work, cold working effects or strain glass phenomena are not the cases observed here. The non-manifestation of DSC peaks in some heat treatment conditions is associated with chemical effects, and potentially internal strain effects due to the precipitates [36]. The lack of perceptible forward and reverse martensitic transformations in the DSC experiments is mostly associated with suppressed transformation temperatures due to Ni staying in solution, thus requiring

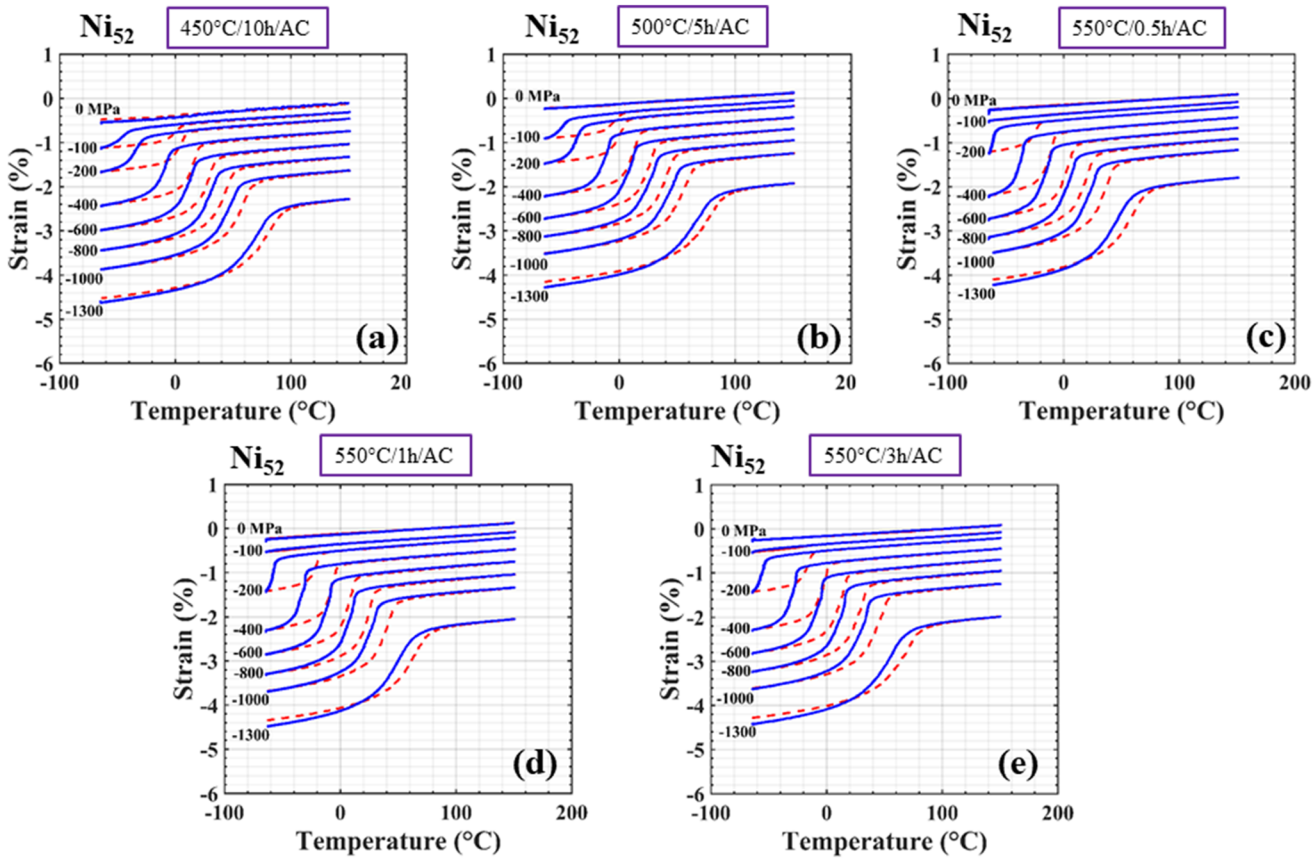

Fig. 9 Compressive constant force thermal cycling responses for the $Ni_{52}Ti_{40}Hf_8$ alloy aged at **a** 450 °C/10 h/AC, **b** 500 °C/5 h/AC, **c** 550 °C/0.5 h/AC, **d** 550 °C/1 h/AC, and **e** 550 °C/3 h/AC. Only the 2nd cycle from some stress levels is shown

further undercooling for the transformation to occur. This is the case for the homogenized heat treatment (1050 °C/24 h/GQ) for the 51–52Ni alloys. The low-temperature limit of − 150 °C for the DSC instrument used was not sufficiently low to promote a full phase transformation. Hence, no peaks were observed in the DSC in the homogenized condition as the transformation takes place in a much lower temperature range unattainable by the DSC instrument.

With aging heat treatments, the precipitation effects take place and manifest in several ways. The H-phase precipitates nucleate and grow, as revealed by the TEM micrographs of Figs. 4 and 5. Generally, these precipitates result in transformation temperature shifts due to change in the chemical composition of the transforming matrix. The H-phase precipitates are Ni and Hf rich, and as the precipitation occurs, they consume Ni from the matrix and decrease the overall matrix Ni content, thus raising the transformation temperatures. This effect is clearly seen in Fig. 1 by the appearance/shift of DSC peaks to higher temperatures after aging, ultimately substantiating the occurrence of martensitic transformation. This is further corroborated by the fully developed hysteresis loops of Figs. 6–9, even for cases where the DSC curves showed very broad and hardly discernable peaks (e.g., the 450 °C/10 h aging condition of Fig. 1a). However, there are cases where even after aging no peaks were developed in the DSC. For example, the 51Ni alloy (Fig. 1b) showed only one heat treatment condition (550 °C/3 h) with clear peaks indicative of the martensitic transformation. The martensite peak for this aging condition occurred at a low value of − 120 °C. It is possible that for other aging conditions this peak occurs at temperatures even lower than this and was not detected due to the lower limit of the instrument (− 150 °C). Thus, the material remained austenitic throughout the DSC temperature range used. This plausible trend is reflected in the thermomechanical data of Fig. 7 and Fig. 11 where the maximum transformation temperatures were obtained for the 550 °C/3 h aging condition, and all the other aging conditions showed a lower value. The reason for such low values of transformation temperatures is the compounded effect of high Ni concentration in the aged matrix and critical size, interparticle spacing and volume fraction of the H-phase precipitates that were observed in all aging conditions (Fig. 4). Particularly, the strain fields created by the H-phase precipitates can inhibit

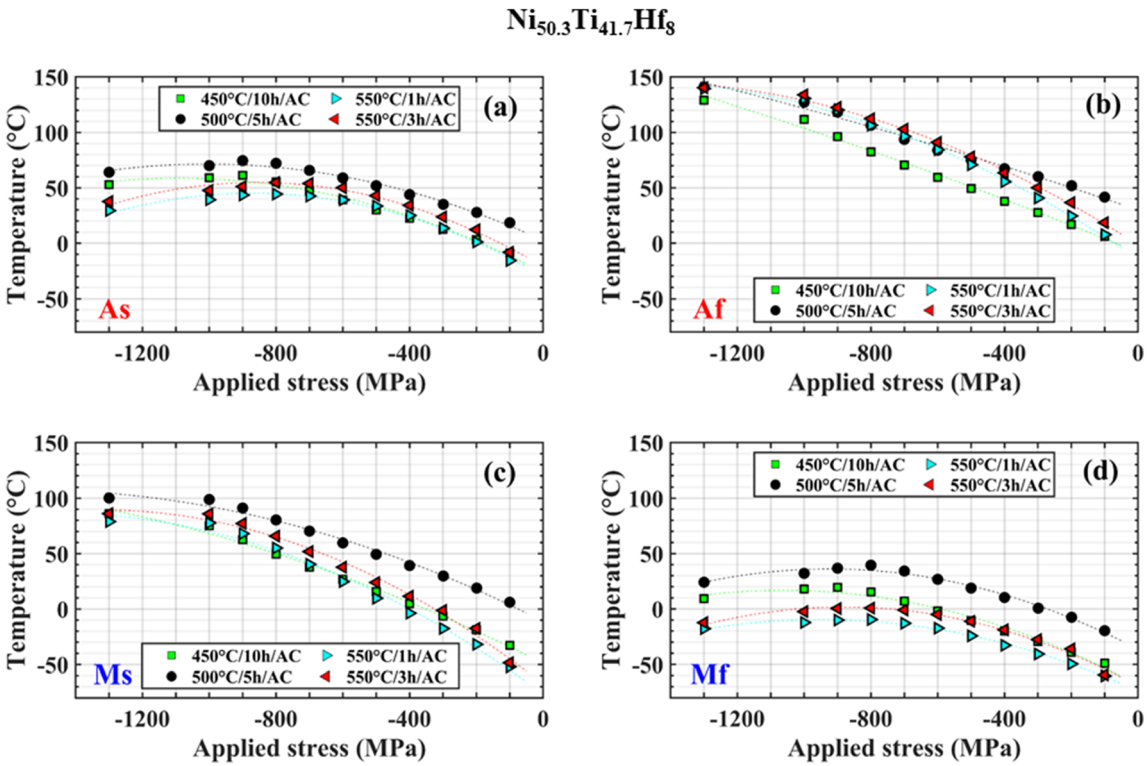

Fig. 10 $Ni_{50.3}Ti_{41.7}Hf_8$ transformation temperatures as a function of applied stress corresponding to the second thermal cycle from the constant force thermal data. **a** Austenite start (A_s), **b** austenite finish (A_f), **c** martensite start (M_s), and **d** martensite finish (M_f)

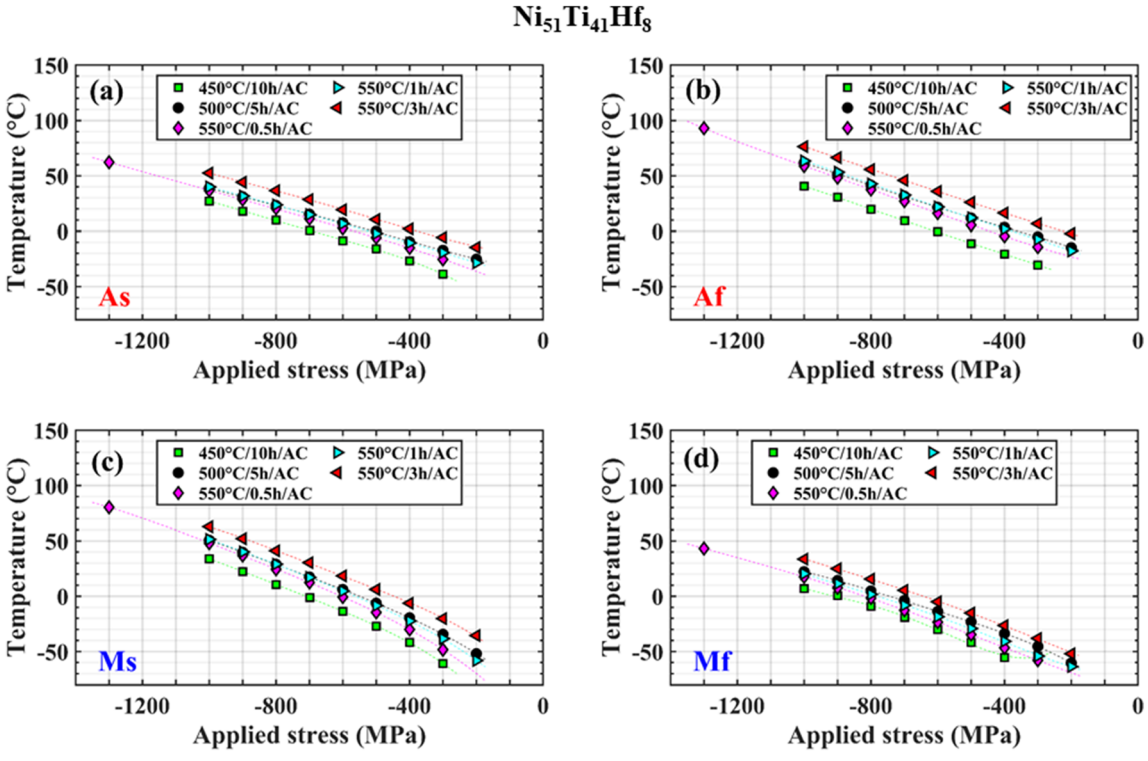

Fig. 11 $Ni_{51}Ti_{41}Hf_8$ transformation temperatures as a function of applied stress corresponding to the second thermal cycle from the constant force thermal data. **a** Austenite start (A_s), **b** austenite finish (A_f), **c** martensite start (M_s), and **d** martensite finish (M_f)

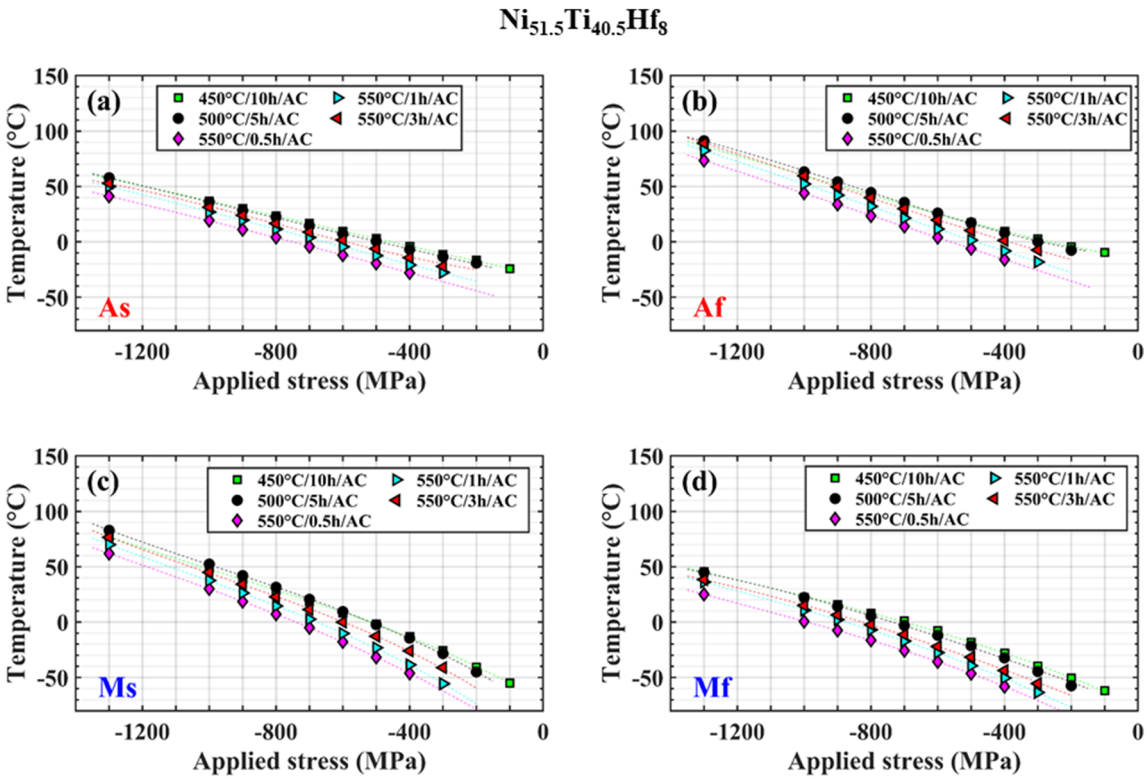

Fig. 12 $Ni_{51.5}Ti_{40.5}Hf_8$ transformation temperatures as a function of applied stress corresponding to the second thermal cycle from the constant force thermal data. **a** Austenite start (A_s), **b** austenite finish (A_f), **c** martensite start (M_s), and **d** martensite finish (M_f)

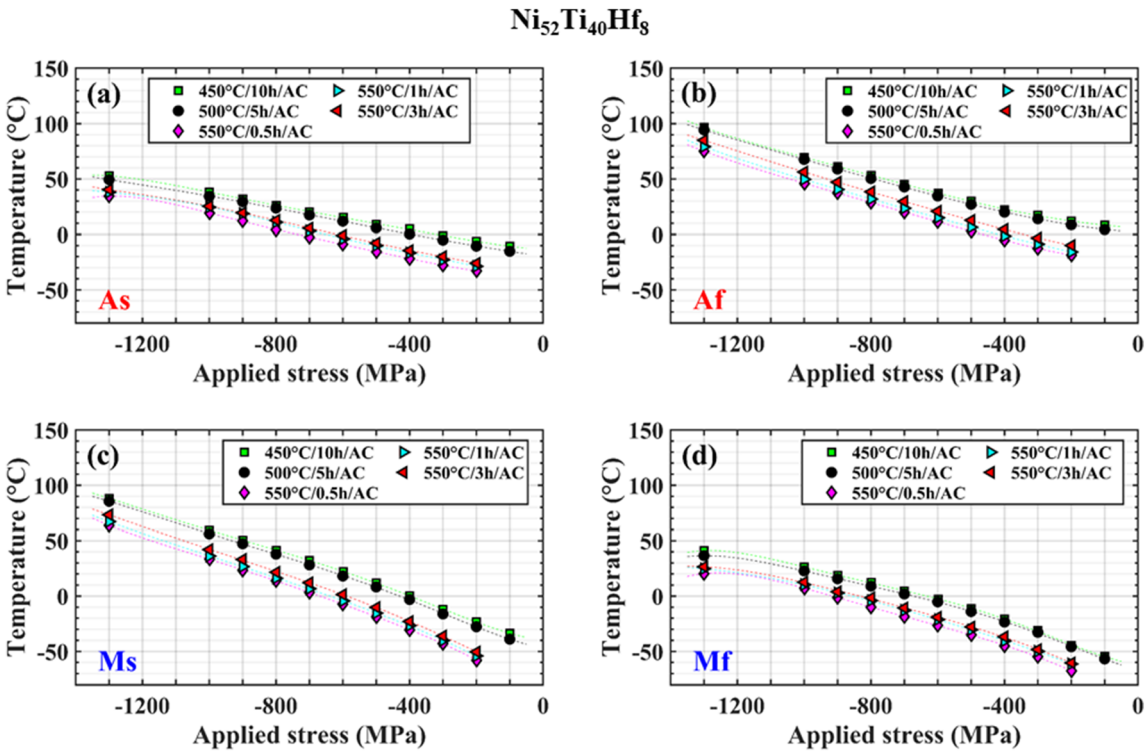

Fig. 13 $Ni_{52}Ti_{40}Hf_8$ transformation temperatures as a function of applied stress corresponding to the second thermal cycle from the constant force thermal data. **a** Austenite start (A_s), **b** austenite finish (A_f), **c** martensite start (M_s), and **d** martensite finish (M_f)

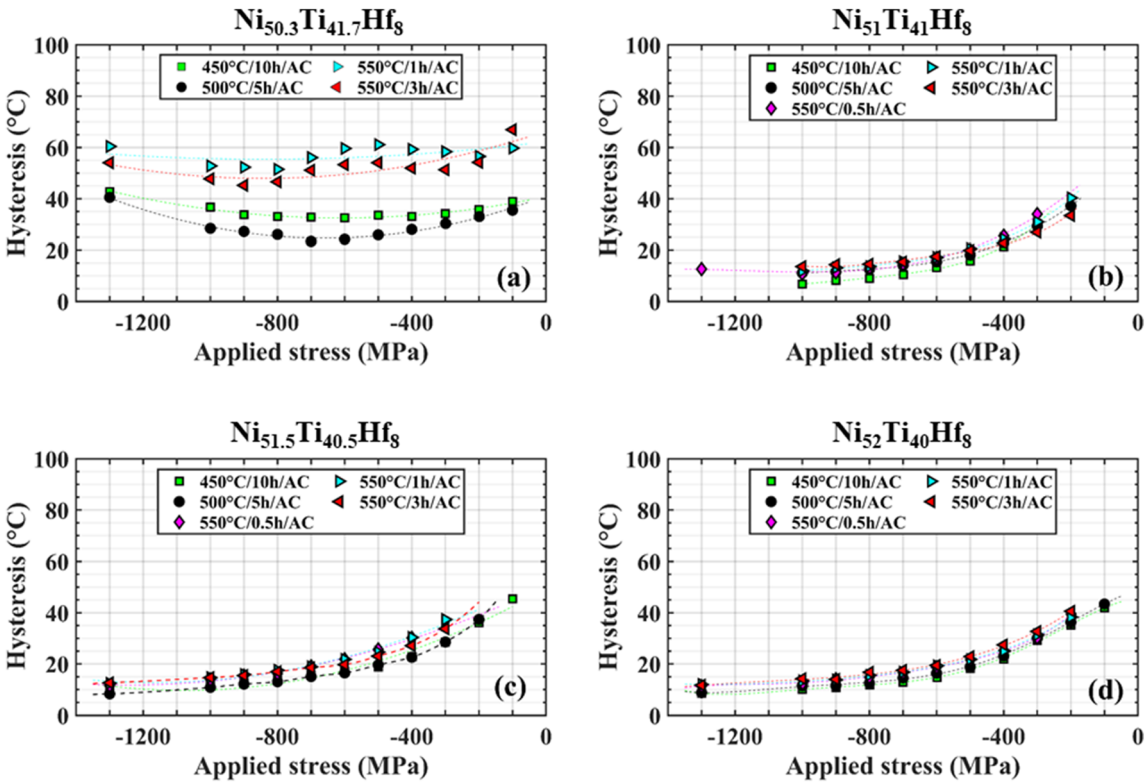

Fig. 14 Thermal hysteresis as a function of applied stress for **a** $Ni_{50.3}Ti_{41.7}Hf_8$, **b** $Ni_{51}Ti_{41}Hf_8$, **c** $Ni_{51.5}Ti_{40.5}Hf_8$, and **d** $Ni_{52}Ti_{40}Hf_8$ (at.%) alloy

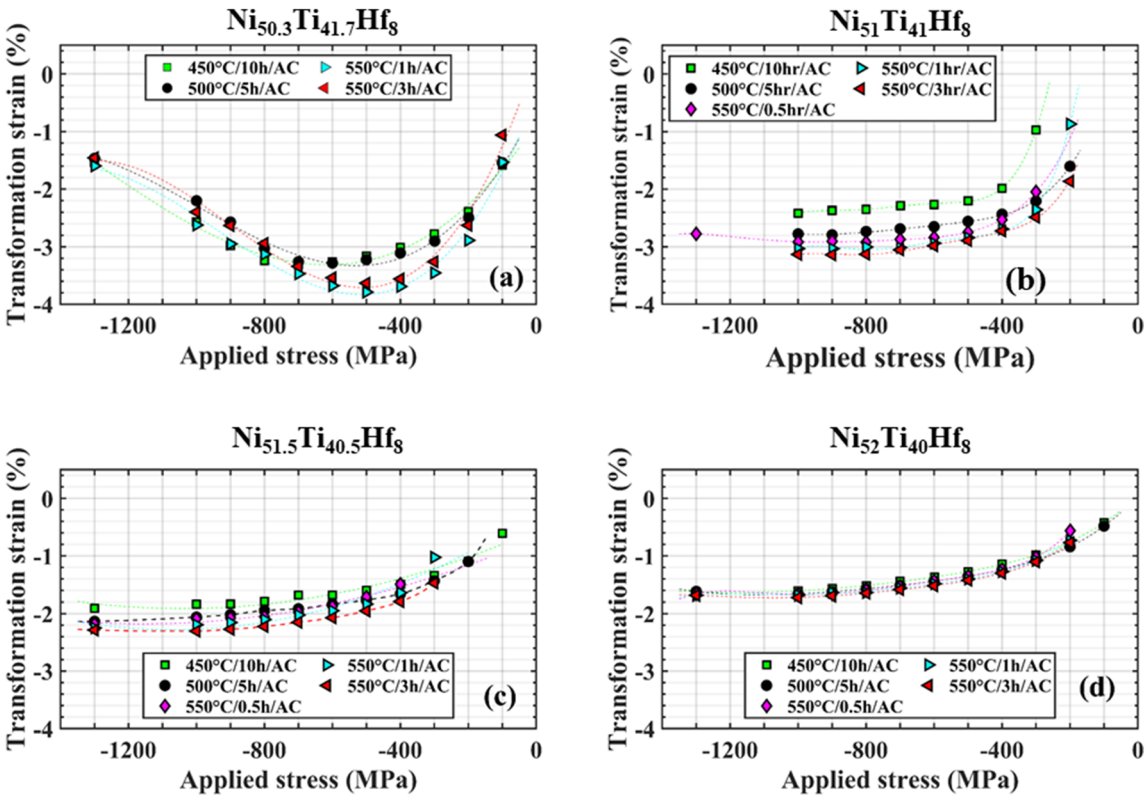

Fig. 15 Transformation strain as a function of applied stress for **a** $Ni_{50.3}Ti_{41.7}Hf_8$, **b** $Ni_{51}Ti_{41}Hf_8$, **c** $Ni_{51.5}Ti_{40.5}Hf_8$, and **d** $Ni_{52}Ti_{40}Hf_8$ (at.%) alloy

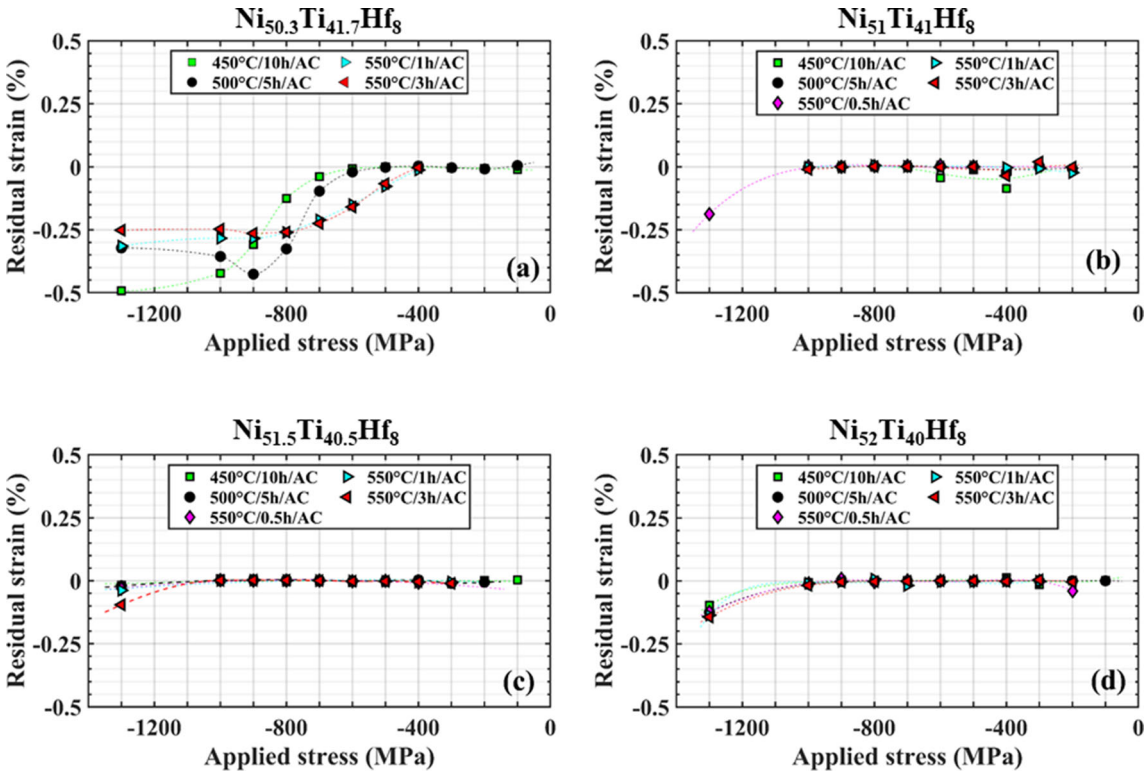

Fig. 16 Residual strain in martensite as a function of applied stress for **a** $Ni_{50.3}Ti_{41.7}Hf_8$, **b** $Ni_{51}Ti_{41}Hf_8$, **c** $Ni_{51.5}Ti_{40.5}Hf_8$, and **d** $Ni_{52}Ti_{40}Hf_8$ (at.%) alloy

the martensite from nucleating [25, 36–38] until a sufficient undercooling or stress is applied (Fig. 7). This compounded effect agrees with the aging study of Ni-rich NiTi single crystals with Ni_4Ti_3 precipitates [39], and warrants further investigation to isolate the two effects.

The 51.5Ni alloy exhibited DSC peaks at the two lower aging temperatures and none for the 550 °C heat treatments. This depression of martensitic transformation at low aging times or higher aging temperatures has also been reported earlier in similar alloy families [36, 37]. Again, once a load was applied (Fig. 8), the combined effects of shifting the transformation temperatures and the stabilization of martensite from the applied load resulted in full hysteresis loops.

The role of the H-phase precipitates in strengthening is also manifested in the hardness data of Fig. 3. In the 50.3Ni low Ni content alloy, precipitation strengthening is not effective since heterogeneous nucleation and a low density of intragranular H-phase precipitates occur with aging (Fig. 5a1). This type of precipitate distribution results in lower hardness which gets worse with aging at higher temperatures (Fig. 3a) where coarsening of precipitates and increase in the interparticle distance become less effective for precipitate hardening. On the other hand, the 51Ni alloy (Fig. 3b) exhibited a more typical precipitate hardening behavior. The lowest hardness was obtained in the homogenized condition (nearly no precipitates), followed by rapid and apparent increase with aging due to the nucleation of a high density of the H-phase precipitates which grew with aging to an appropriate size for optimum precipitate strengthening. Referring back to the TEM microstructures in Fig. 4, there is only slight growth and coarsening of the H-phase with higher aging time/temperature, leading to near uniform hardness, with only a small softening at the last aging condition. Clearly, as shown by Figs. 3 and 5, uniform precipitation of the H-phase through heat treatment requires an optimum (or minimum) (Ni + Hf) content, which is satisfied by increasing the Ni from 50.3 to 51 at.%. Logically, this is reasonable and has been observed in several other studies. Amin-Ahmadi et al. [9] reported heterogeneous nucleation of the H-phase precipitates in a 50.3Ni alloy with 6 and 8.5 Hf content (similar to the current work), which then transitioned to a homogeneous precipitation by increasing the Hf content to 9 at.%. In our work, the same effect is observed by adding more Ni rather than more Hf. Other alloys with a much higher Ni content were also studied by Hornbuckle et al. [40], showing the effect of dilute solute additions of Hf on the formation of the H-phase. In this work, adding more Ni promoted the uniform precipitation, which resulted in increased hardness. Adding even more Ni, as in 51.5Ni and 52Ni alloys, resulted in a near constant hardness (Fig. 3).

This is attributed to solution strengthening and precipitate hardening by dense uniform nm-size H-phase even in the as-homogenized condition, with no significant change in hardness with different aging heat-treatments.

The thermomechanical responses present a consistent trend with the above observations. First, the transformation strains decreased with the added Ni (Fig. 15) due to aging induced formation of non-transforming H-phase precipitates, resulting in reduced overall transforming volume (martensite to austenite) that contributes to strain generation (see Fig. 5). As a result, the maximum transformation strains decreased by nearly 46% (strains decreased from 3.7 to 1.7%) by increasing the Ni content from 50.3 to 52 at.%. Second, the effect of aging heat treatments is more pronounced for the lower Ni-containing alloys. Clearly, both the 50.3Ni and the 51Ni alloys exhibited a range of transformation strains depending on the aging conditions. Commensurate with the hardness data, microstructural changes that occur with aging in these two alloys alter the phase fraction (matrix versus precipitates), precipitate size, and precipitate spacing, which are reflected in the hardening and softening behavior. On the other hand, for the 51.5Ni and 52Ni alloys, the effect of aging heat treatment on transformation strain is diminished (Fig. 15c, d), likely due to the H-phase fraction reaching a saturation point, which agrees with the high hardness and limited change in hardness with aging conditions (Fig. 3c, d).

Precipitation strengthening also play an important role on stabilizing the actuation response. It is known that the nanometer sized H-phase precipitates act as a barrier to dislocation motion, resulting in stronger and more stable alloys [9]. The 50.3Ni alloy, with ineffective precipitate strengthening (Fig. 5a1–a3), exhibits maximum transformation strains at stress levels around 500 MPa followed by a transformation strain decrease at higher stresses (Fig. 15). Such trend is typical in alloys with no or insufficient strengthening mechanisms, where irreversible mechanisms such as dislocation generation and retained martensite take over at higher stresses at the expense of reversible phase transformation. This is further illustrated in Fig. 16a which shows a rapid accumulation of residual strains past a critical stress of 500–600 MPa. In the higher Ni counterparts, the solid solution and precipitation strengthening is enough to delay irrecoverable mechanisms even at high stresses. Thus, there is nearly zero residual strain up to 1000 MPa as shown in Fig. 16b–d, followed by some residual strain development at 1300 MPa, but it never reaches the high magnitudes that were obtained in the 50.3Ni. This strengthening results in transformation strains that do not reach a maximum and then decrease due to the activation of irrecoverable mechanisms, but rather increase gradually with added stress as the stress produces additional favorable martensite orientation.

Finally, we note that the above mechanisms and trends also translate to the hysteresis behavior. Thermal hysteresis is shown to generally remain constant or increase with added stress in the 50.3Ni alloy but decreases significantly with stress in the higher Ni alloys (Fig. 14). This is commonly seen in similar alloys [28, 29], where Ni-lean or stoichiometric alloys exhibit wider hysteresis with increasing stress commensurate with buildup of residual strains, while the relatively Ni richer alloys tend to exhibit a narrower hysteresis with added stress.

Concluding Remarks

A set of NiTi-8Hf (at.%) alloys with varying Ni content were evaluated for their shape memory properties. Four alloys with a Ni content of 50.3, 51, 51.5 and 52 at.% were produced and their thermomechanical behavior was assessed using uniaxial constant force thermal cycling (UCFTC) in compression and differential scanning calorimetry (DSC), while microstructures were evaluated using transmission electron microscopy (TEM). The following conclusions can be made:

- Aging NiTi-8Hf alloys at temperatures between 450 and 550 °C produced nano-sized H-phase precipitates. These precipitates varied in size ranging from 12 to 76 nm depending on the Ni content and aging conditions. A threshold Ni + Hf content was required to transition from a heterogeneous nucleation of the H-phase precipitates (e.g., in the 50.3Ni alloy) to a more uniform and homogeneous distribution (e.g., in the 51–52Ni alloys).
- DSC measurements were used as an initial procedure to detect the martensitic transformation. However, some alloy conditions did not show any enthalpy peaks in DSC, but full hysteresis loops were present when the alloys were tested under applied loads. In these conditions, the effect of Ni-concentration in the aged matrix, the precipitates size and volume fraction, and the Ni/Ti ratios were responsible for suppressing the martensitic transformation. The suppressed transformation was revealed by the application of a load during thermal cycling and could possibly be revealed by going to lower temperatures during cycling in the DSC.
- Thermomechanical responses show that (50.3-52Ni)-Ti-8Hf alloy can be tailored to produce promising low temperature actuation strains of as high as 3.7% at 500 MPa in compression. When thermal cycling under load, dimensional stability was largely affected by the H-phase precipitates, showing large accumulation of residual strains in the alloy with heterogeneously formed precipitates, while exhibiting very

stable response in alloys with a high density of fine and homogenous precipitate distribution.

Acknowledgements Funding from the NASA Aeronautics Research Mission Directorate (ARMD) Transformational Tools and Technologies (TTT) project is gratefully acknowledged. O.B. thanks R.D Noebe for help with alloy formulation.

References

1. Benafan O, Moholt MR, Bass M, Mabe JH, Nicholson DE, Calkins FT (2019) Recent advancements in rotary shape memory alloy actuators for aeronautics. Shape Memory Superelast 5(4):415–428
2. Casalena L, Bucsek AN, Pagan DC, Hommer GM, Bigelow GS, Obstalecki M, Noebe RD, Mills MJ, Stebner AP (2018) Structure-property relationships of a high strength superelastic NiTi–1Hf alloy. Adv Eng Mater 20(9):1800046
3. DellaCorte C, Stanford MK, Jett TR (2015) Rolling contact fatigue of superelastic intermetallic materials (SIM) for use as resilient corrosion resistant bearings. Tribol Lett 57(3):26
4. Mills SH, Noebe RD, Dellacorte C, Amin-Ahmadi B, Stebner AP (2020) Development of nickel-rich nickel–titanium–hafnium alloys for tribological applications. Shape Memory Superelast 6(3):311–322
5. O. Benafan, G.S. Bigelow, R.D. Noebe, A. Garg, D.J. Gaydosh (2017) On the Processability and Scale-Up of NiTi-20Hf High Temperature Shape Memory Alloys, The International Conference on Shape Memory and Superelastic Technologies (SMST 2017), San Diego, CA
6. C. DellaCorte (2019) Dimensionally Stable Shape Memory Alloys for Mechanical Engineering Applications: The Other Side of Superelastics, Advanced Materials & Processes, pp. 43–47
7. Benafan O, Bigelow GS, Garg A, Noebe RD, Gaydosh DJ, Rogers RB (2021) Processing and scalability of NiTiHf high temperature shape memory alloys shap. Mem Superelast. https://doi.org/10.1007/s40830-020-00306-x
8. T. Duerig (2017) Superelastic devices made from NiTiHf alloys using powder metallurgical techniques, U.S. Patent Application No. 15/272,340
9. Amin-Ahmadi B, Gallmeyer T, Pauza JG, Duerig TW, Noebe RD, Stebner AP (2018) Effect of a pre-aging treatment on the mechanical behaviors of $Ni_{50.3}Ti_{49.7-x}Hf_x$ ($x \leq 9$ at.%) Shape memory alloys. Scripta Materialia 147:11–15
10. Benafan O, Bigelow GS, Garg A, Noebe RD (2019) Viable low temperature shape memory alloys based on Ni-Ti-Hf formulations. Scripta Mater 164:115–120
11. F. Calkins, A. Fassmann, P. Vijgen, D. Nicholson, M. Bass, O. Benafan, D. Gaydosh, G. Bigelow, R. Noebe, Shape memory alloy reconfigurable technology-vortex generators (SMART-VG) can reduce fuel consumption and improve aircraft efficiency, Advanced Materials & Processes, 2020, pp. 60–62.
12. D. Angst, P. Thoma, M. Kao (1995) The effect of hafnium content on the transformation temperatures of $Ni_{49}Ti_{51-x}Hf_x$. Shape memory alloys. J Phys IV 5(C8), C8-747–C8-752.
13. M. Prasher, D. Sen, R. Tewari, P. Krishna, P. Babu, M. Krishnan (2020) Effect of Hf solute addition on the phase transformation behavior and hardness of a Ni-rich NiTi alloy. Mater Chem Phys 122890
14. Umale T, Salas D, Tomes B, Arroyave R, Karaman I (2019) The effects of wide range of compositional changes on the martensitic transformation characteristics of NiTiHf shape memory alloys. Scripta Mater 161:78–83
15. Frenzel J, George EP, Dlouhy A, Somsen C, Wagner MFX, Eggeler G (2010) Influence of Ni on martensitic phase transformations in NiTi shape memory alloys. Acta Mater 58(9):3444–3458
16. D.N. AbuJudom II, P.E. Thoma, M.-Y. Kao, D.R. Angst (1992) High transformation temperature shape memory alloy, Patent Number 5,114,504
17. Potapov PL, Shelyakov AV, Gulyaev AA, Svistunov EL, Matveeva NM, Hodgson D (1997) Effect of Hf on the structure of Ni-Ti martensitic alloys. Mater Lett 32(4):247–250
18. Dalle F, Perrin E, Vermaut P, Masse M, Portier R (2002) Interface mobility in $Ni_{49.8}Ti_{42.2}Hf_8$ shape memory alloy. Acta Materialia 50(14):3557–3565
19. Dalle F, Despert G, Vermaut P, Portier R, Dezellus A, Plaindoux P, Ochin P (2003) $Ni_{49.8}Ti_{42.2}Hf_8$ shape memory alloy strips production by the twin roll casting technique. Mater Sci Eng: A 346(1):320–327
20. Kockar B, Karaman I, Kim JI, Chumlyakov Y (2006) A method to enhance cyclic reversibility of NiTiHf high temperature shape memory alloys. Scripta Mater 54(12):2203–2208
21. A.A. Simon, Shape memory response and microstructural evolution of a severe plastically deformed high temperature shape memory alloy (NiTiHf), Texas A&M University, 2006.
22. Wojcik CC (2009) Properties and heat treatment of high transition temperature Ni-Ti-Hf alloys. J Mater Eng Perform 18(5–6):511–516
23. Tong Y, Chen F, Tian B, Li L, Zheng Y (2009) Microstructure and martensitic transformation of $Ti_{49}Ni_{51-x}Hf_x$ high temperature shape memory alloys. Mater Lett 63(21):1869–1871
24. König D, Zarnetta R, Savan A, Brunken H, Ludwig A (2011) Phase transformation, structural and functional fatigue properties of Ti–Ni–Hf shape memory thin films. Acta Mater 59(8):3267–3275
25. Amin-Ahmadi B, Pauza JG, Shamimi A, Duerig TW, Noebe RD, Stebner AP (2018) Coherency strains of H-phase precipitates and their influence on functional properties of nickel-titanium-hafnium shape memory alloys. Scripta Mater 147:83–87
26. Soares RL, Castro WBD (2019) Effects of composition on transformation temperatures and microstructure of Ni-Ti-Hf shape memory alloys. REM-Int Eng J 72(2):227–235
27. Yang F, Coughlin DR, Phillips PJ, Yang L, Devaraj A, Kovarik L, Noebe RD, Mills MJ (2013) Structure analysis of a precipitate phase in an Ni-rich high-temperature NiTiHf shape memory alloy. Acta Mater 61(9):3335–3346
28. Bigelow G, Benafan O, Garg A, Lundberg R, Noebe R (2019) Effect of composition and applied stress on the transformation behavior in NiXTi80−XZr20 shape memory alloys. Shape Memory Superelast 5(4):444–456
29. Hamilton RF, Sehitoglu H, Chumlyakov Y, Maier H (2004) Stress dependence of the hysteresis in single crystal NiTi alloys. Acta Mater 52(11):3383–3402
30. Babacan N, Bilal M, Hayrettin C, Liu J, Benafan O, Karaman I (2018) Effects of cold and warm rolling on the shape memory response of $Ni_{50}Ti_{30}Hf_{20}$ high-temperature shape memory alloy. Acta Mater 157:228–244
31. Lin HC, Wu SK, Chou TS, Kao HP (1991) The effects of cold rolling on the martensitic transformation of an equiatomic TiNi alloy. Acta Metall Mater 39(9):2069–2080
32. Zhang J, Xue D, Cai X, Ding X, Ren X, Sun J (2016) Dislocation induced strain glass in $Ti_{50}Ni_{45}Fe_5$ alloy. Acta Mater 120:130–137
33. Ren X (2014) Strain glass and ferroic glass–Unusual properties from glassy nano-domains. Physica Status Solidi 251(10):1982–1992

34. Wang D, Zhang Z, Zhang J, Zhou Y, Wang Y, Ding X, Wang Y, Ren X (2010) Strain glass in Fe-doped Ti–Ni. Acta Mater 58(18):6206–6215
35. Monroe JA, Raymond JE, Xu X, Nagasako M, Kainuma R, Chumlyakov YI, Arroyave R, Karaman I (2015) Multiple ferroic glasses via ordering. Acta Mater 101:107–115
36. Kornegay SM, Kapoor M, Hornbuckle B, Tweddle D, Weaver ML, Benafan O, Bigelow GS, Noebe RD, Thompson GB (2020) Influence of H-phase Precipitation on the Microstructure and Functional and Mechanical Properties in a Ni-rich NiTiZr Shape Memory Alloy. Mater Sci Eng, A 801:140401
37. Evirgen A, Basner F, Karaman I, Noebe RD, Pons J, Santamarta R (2012) Effect of aging on the martensitic transformation characteristics of a Ni-rich NiTiHf high temperature shape memory alloy. Funct Mater Lett 5(04):1250038
38. Coughlin DR, Casalena L, Yang F, Noebe RD, Mills MJ (2016) Microstructure–property relationships in a high-strength 51Ni–29Ti–20Hf shape memory alloy. J Mater Sci 51(2):766–778
39. Panchenko EY, Chumlyakov YI, Kireeva I, Ovsyannikov A, Sehitoglu H, Karaman I, Maier Y (2008) Effect of disperse Ti_3N_4 particles on the martensitic transformations in titanium nickelide single crystals. Phys Met Metallogr 106(6):577
40. Hornbuckle B, Noebe R, Thompson G (2015) Influence of Hf solute additions on the precipitation and hardenability in Ni-rich NiTi alloys. J Alloy Compd 640:449–454